CRYSTAL GROWTH & DESIGN

Article

pubs.acs.org/crystal

A New Isomeric Porous Coordination Framework Showing Single-Crystal to Single-Crystal Structural Transformation and Preferential Adsorption of 1,3-Butadiene from C4 Hydrocarbons

Published as part of a Crystal Growth and Design virtual special issue on Crystal Engineering of Nanoporous Materials for Gas Storage and Separation

Zi-Ming Ye,[†,#] Chun-Ting He,[†,#] Yan-Tong Xu,[†] Rajamani Krishna,[‡] Yi Xie,[†] Dong-Dong Zhou,[†] Hao-Long Zhou,[†] Jie-Peng Zhang,*[,†] and Xiao-Ming Chen*[,†]

[†]MOE Key Laboratory of Bioinorganic and Synthetic Chemistry, School of Chemistry, Sun Yat-Sen University, Guangzhou 510275, China

[‡]Van't Hoff Institute for Molecular Sciences, University of Amsterdam, Science Park 904, 1098 XH Amsterdam, The Netherlands

Supporting Information

ABSTRACT: Reaction of $Zn(NO_3)_2$ and 4-(3,5-dimethyl-1*H*-pyrazol-4-yl) benzoic acid (H_2mpba) in a mixed solvent of methanol and toluene gives a new supramolecular isomer for [Zn(Hmpba)$_2$]·guest (**1·g**). Single crystal X-ray diffraction analysis showed that **1·g** possesses a similar local coordination structure with the three known [Zn(Hmpba)$_2$]·guest isomers with 4-fold interpenetrated **dia** topologies (dissimilar interpenetration directions, void ratio varies from 0% to 28%), but displays a rare 4-connected **afw** topology consisting of three- and seven-membered rings, and remains a large void ratio of 36% even after 4-fold interpenetration. Interestingly, **1·g** can undergo obvious framework contraction of 8.5% in the single-crystal to single-crystal manner upon guest removal to give [Zn(Hmpba)$_2$] (**1′**). Comparison of the single-crystal structures of **1·g** and **1′** showed that the structural transformation arises mainly from ligand conformation change. Single-component N_2, CO_2, and C4 hydrocarbon gas adsorption measurements for **1′** show different isotherm steps and gate-opening pressures, in which 1,3-butadiene is the lowest in the five C4 hydrocarbons, likely because of it has the smallest molecular cross-section area. Breakthrough simulations on mixed C4 hydrocarbons showed that 1,3-butadiene is preferentially adsorbed from other C4 hydrocarbons.

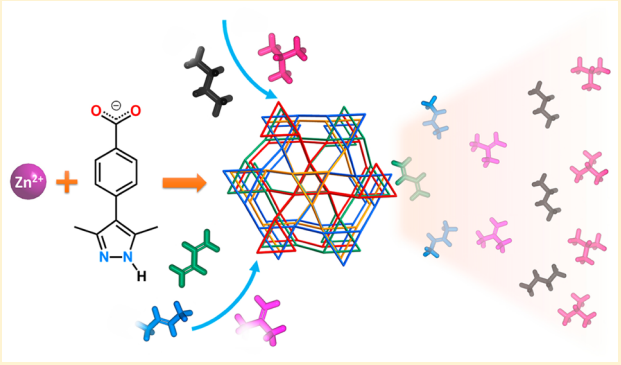

INTRODUCTION

Porous coordination polymers (PCPs) or metal organic frameworks (MOFs), being constructed by metal ions and organic linkers, have attracted great interest for their large porosity, ordered structures, and remarkable framework flexibilities, as well as a variety of potential applications such as catalysis,[1−3] drug delivery,[4−8] gas separation,[9−16] and storage.[14,17−21] The structural transformation or dynamism of flexible MOFs can be observed at the molecular level by diffraction techniques, although preservation of sample single-crystallinity or observation of single-crystal to single-crystal (SCSC) transformation is always challenging because the involved large mechanical strains tend to crack the large crystals.[22] Flexible MOFs can show very different structural dynamism such as gate-opening actions toward similar yet different guests,[23−28] which might be useful for enhancing gas separation performance.[29−32] However, the flexibilities in MOFs are rather difficult to design and control.[33]

The difficulty of controlling properties/flexibilities of MOFs partially arises from the uncertain synthesis of desired framework structures and unclear structure−property relationship. While some useful crystal-engineering strategies have been developed, as exemplified by the successful designs and syntheses of a variety of classical MOFs,[12,34,35] it is still very difficult to predict or control the chemical composition of a MOF in many occasions.[36−39] Even for a given chemical composition, there are usually several different framework structures, which are known as supramolecular isomerism.[40−43] Although supramolecular isomerism means uncertain synthesis and impure products, supramolecular isomers are beneficial in the analyses of structure−property relationships because the composition differences of materials are avoided.

Received: January 23, 2017
Revised: February 26, 2017
Published: March 9, 2017

DOI: 10.1021/acs.cgd.7b00100
Cryst. Growth Des. 2017, 17, 2166−2171

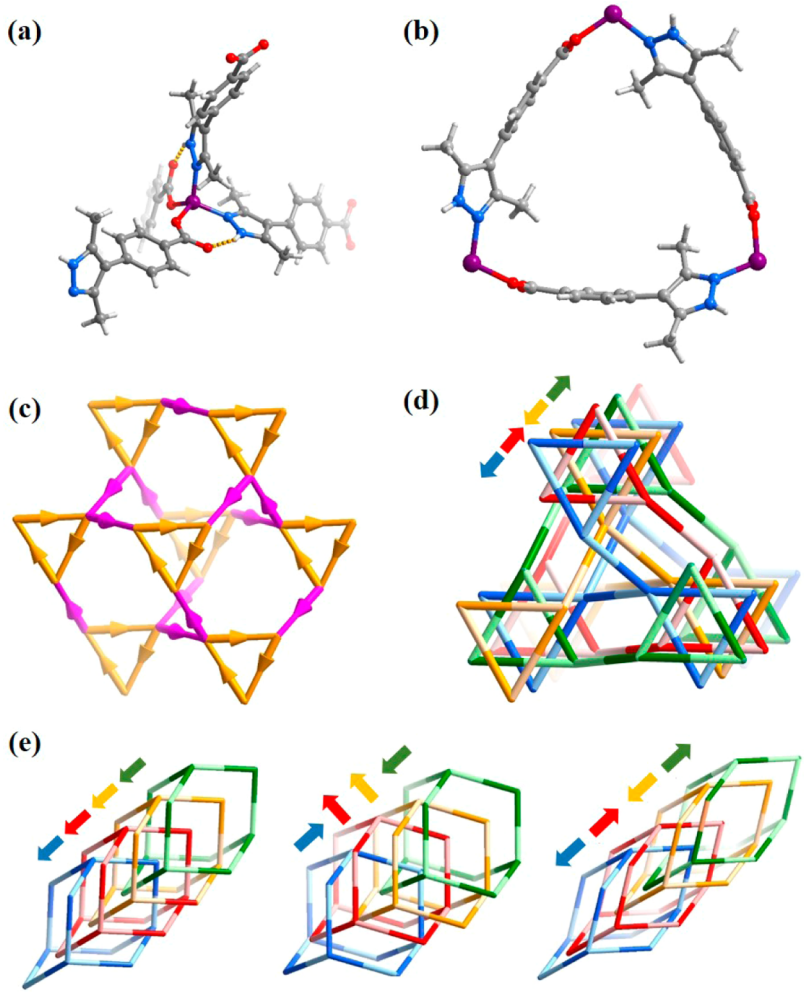

Figure 1. (a) The coordination environment, (b) three-membered ring, (c) chiral and polar **afw** topology (the pyrazole to carboxylate vectors of the linkers are highlighted as arrows; the three-membered rings and 3_1 helices are highlighted in orange and pink, respectively), and (d) interpenetration mode of **1·g**. (e) Three topological isomers of **1·g** possessing the **dia** topology with different interpenetration directions.[46]

The ditopic ligand 4-(3,5-dimethyl-1*H*-pyrazol-4-yl)benzoic acid (H_2mpba) can react with Zn(II) salts to give a variety of MOF structures.[44−47] In *N*,*N*-diethylformamide at 140 °C, the product is a MOF-5 typed, rigid structure $[Zn_4(\mu_4\text{-}O)(mpba)_3]$ based on octahedral $[Zn_4(\mu_4\text{-}O)(\mu\text{-}RCOO)_3(\mu\text{-}Rpz)_3]$ clusters and fully deprotonated $mpba^{2-}$ linkers, which possesses a three-dimensional (3D) pore system with a diameter of 8.5 Å.[44] When the reaction temperature is decreased to 120 °C and using mixed *N*,*N*-dimethylacetamide/methanol as solvent, the product is a pillared-column type rigid 3D framework [Zn(mpba)] (MAF-X8) based on infinite $Zn(\mu\text{-}RCOO)(\mu\text{-}Rpz)$ columns and $mpba^{2-}$ pillars, which possesses large one-dimensional (1D) channels with a size of 8.8 Å.[44] By decreasing the synthesis temperature to 100 °C and using mixed ethanol/water as a neutral solvent, the ditopic ligand can partially deprotonate on the carboxylic group and coordinate with Zn(II) in a molar ratio of 2:1 to form polar 3D 4-connected **dia** networks $[Zn(Hmpba)_2]$ based on mononuclear $Zn(RCOO)_2(Rpz\text{-}H)_2$ (Rpz-H = neutral pyrazole group) nodes with 4-fold interpenetration. Interestingly, the polar **dia** networks can arrange in different directions to form three interpenetration-direction isomers, giving rise to drastically different pore systems (3D, zero-dimensional (0D), and nonporous for α-$[Zn(Hmpba)_2]$, β-$[Zn(Hmpba)_2]$, and γ-$[Zn(Hmpba)_2]$, respectively) and framework dynamisms.[46] Nevertheless, their single-crystallinity could not be maintained during the guest-induced structural transformations, so that their transformed structures can be only explicated by powder X-ray diffraction (PXRD) and computational simulation.[46]

In principle, except for the extraordinary interpenetration-direction isomers, $[Zn(Hmpba)_2]$ might also show the more common type of supramolecular isomerism based on the differences of interpenetration numbers and/or topologies.[40−43] With this expectation, we performed a further study for the self-assembly of H_2mpba and Zn(II) salts, and discovered a new supramolecular isomer for $[Zn(Hmpba)_2]$ showing a rare **afw** topology, by using toluene as a template. Similar with the **dia** isomers, the new compound exhibits framework flexibility during guest adsorption/desorption processes. However, because of the difference in topology, the **afw** isomer has a larger porosity. We also successfully obtained the single-crystal structure for its guest-free state and found different gating behaviors toward N_2, CO_2, and various C4 hydrocarbons, which might be useful for enrichment of 1,3-butadiene from C4 hydrocarbons.[48]

DOI: 10.1021/acs.cgd.7b00100
Cryst. Growth Des. 2017, 17, 2166−2171

EXPERIMENTAL SECTION

Materials and Methods. All reagents were commercially available and used without purification except otherwise specified. H_2mpba was synthesized according to the literature method.[44,49] Elemental analyses (EA) (C, H, N) were performed by a Vario El elemental analyzer. PXRD was performed on a D8 DAVANCI X-ray powder diffractometer (Cu Kα). Thermogravimetry (TG) analyses were carried out with a TGA Q50 system. Each sample was heated to 700 °C at a rate of 5 °C·min^{-1} under N_2 atmosphere. N_2 and CO_2 gas sorption isotherms were measured by using an automatic volumetric adsorption apparatus Micromertics ASAP 2020M. C4 hydrocarbon sorption isotherms were measured by using an automatic volumetric adsorption apparatus BELSORP-max. An amount of ca. 100−200 mg as-synthesized sample was placed in a sample tube and then heated at 150 °C in dynamic vacuum for 10 h to remove the remnant solvent molecules before isotherm measurement.

Synthesis of δ-[Zn(Hmpba)$_2$]·guest (MCF-42δ or 1·g). A mixture of MeOH (4.0 mL), toluene (2.0 mL), $Zn(NO_3)_2{\cdot}6H_2O$ (30.0 mg, 0.1 mmol), and H_2mpba (22.0 mg, 0.1 mmol) was sealed in a 15 mL glass vessel and heated at 90 °C for 3 days, and then cooled to room temperature at a rate of 10 °C·h^{-1}. Colorless single crystals were filtered and dried in air (60% yield based on H_2mpba). EA calculated (%) for $[Zn(C_{12}H_{11}N_2O_2)_2]{\cdot}1.05C_7H_8$ ($C_{31.35}H_{30.4}N_4O_4Zn$): C, 63.54; H, 5.17; N, 9.45. Found (%): C, 62.26; H, 5.13; N, 9.31.

Crystal Structure Determination. Single-crystal X-ray diffraction data were collected on an Oxford Gemini S Ultra CCD diffractometer (Cu Kα) and a Bruker SMART APEX CCD diffractometer (Mo Kα). The structures were solved by the direct method and refined by the full-matrix least-squares technique on F^2 using the SHELXTL software package. Hydrogen atoms attached on carbon atoms were placed geometrically, while those attached on nitrogen atoms were located from the residue electron peaks and refined without any restriction. All non-hydrogen atoms of the host framework and disordered guest molecule were refined by using anisotropic thermal parameters. To keep the anisotropic thermal parameters of the disordered toluene atoms within reasonable limits, the displacement components were restrained using ISOR and SIMU instructions. The crystal data and structure refinement results are summarized in Table S1. CCDC 1528960 and 1528961 contain the supplementary crystallographic data for this paper. These data can be obtained free of charge from The Cambridge Crystallographic Data Centre via www.ccdc.cam.ac.uk/data_request/cif.

RESULTS AND DISCUSSION

Synthesis, Structure, and Flexibility. The reaction of $Zn(NO_3)_2$ and H_2mpba in a mixed solvent of methanol and toluene gave a new isomer, namely, δ-[Zn(Hmpba)$_2$]·guest (**1·g**). Single-crystal X-ray diffraction analysis revealed that **1·g** crystallizes in a trigonal space group $R\bar{3}$ (Table S1 and Figure 1). The asymmetric unit consists of one Zn(II) ion, two Hmpba$^-$ ligands, and some disordered guest molecules which are mainly composed of toluene. Each Zn(II) ion is coordinated by two N atoms from two pyrazole groups (Zn−N 1.989(3) Å and 1.995(2) Å) and two O atoms from two carboxylate groups (Zn−O 1.916(2) Å and 1.923(3) Å) to form a distorted tetrahedral geometry (N−Zn−N/O−Zn−O/N−Zn−O 104.7(1)°−115.0(1)°). While deprotonation only occurs on the more acidic carboxylic groups, hydrogen bonds (N−H···O 2.695(3) Å and 2.749(5) Å) between the neutral pyrazol N−H moieties and the uncoordinated carboxylate O atoms can be observed. While the Hmpba$^-$ ligands act as 2-connected linkers and the Zn(II) ions act as 4-connected nodes like the **dia** isomers, they interconnect to form a rare **afw** network with a point symbol of 3.7^5 and a vertex symbol of $3.7.7.7.7_2.7_2$.[50] This topology is unique for its presences of rare three-membered rings and seven-membered rings. It also contains parallelly arranged 3_1 helices, meaning that it is intrinsically chiral. Combination of tetrahedral metal ions (109.5°) and linear ligands obviously cannot fit in the triangular geometry. In **1·g**, this is compensated by a torsion of the ligand along its long axis. After introduction of polar ligands, the **afw** net in **1·g** becomes polar because the polar ligands in the 3_1 helices arrange nearly parallel with the *c*-axis. Similar to its **dia** isomers, **1·g** is also 4-fold interpenetrated. The interpenetration mode of **1·g** can be classified as type IIIa (two pairs nets related by translation and inversion), which produces a mesomeric or centrosymmetric overall structure. There are two types of 1D channels in the structure both running along the crystallographic *c*-axis, which are occupied by disordered toluene molecules. The larger (channel A) and smaller (channel B) ones are gourd-shaped (widest and narrowest cross section diameters of 7.8 and 4.7 Å) and rhombic (cross section area of 5.4 × 6.4 Å^2), respectively (Figure 2a). Compared to the conventional 3D 4-connected **dia** net (0.6495 Å^{-3}), **afw** has a lower topology density (0. 5577 Å^{-3}). Therefore, the void ratio in **1·g** (35.9%) is higher than all the **dia** isomers (0−27.7%).

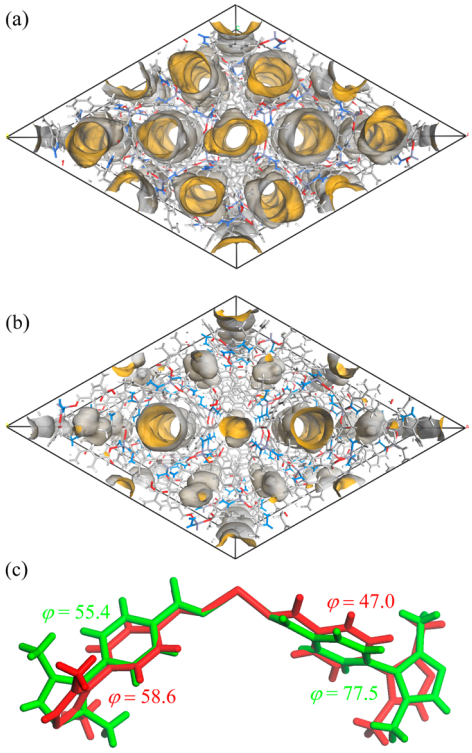

Figure 2. Structural transformation between **1·g** and **1′**. Coordination framework and pore surface structures of (a) **1** and (b) **1′**. (c) Overlap of the asymmetric units of **1·g** (red) and **1′** (green). The dihedral angle between the phenyl ring and the pyrazole ring of a Hmpba$^-$ ligand is defined as φ.

The TG curve of **1·g** exhibits a weight loss of 19.5% from 85 to 150 °C corresponding to the removal of toluene molecules (calculated 18.5%), and then there is a long plateau up to the decomposition temperature of 350 °C (Figure S1). PXRD patterns showed an obvious structural transformation upon guest removal (Figure S2), giving guest-free [Zn(Hmpba)$_2$] (**1′**). By exposing **1′** in toluene vapor, the characteristic PXRD pattern of **1·g** can be restored (Figure S2), indicating that the guest-induced structural transformation between **1·g** and **1′** is reversible.

DOI: 10.1021/acs.cgd.7b00100
Cryst. Growth Des. 2017, 17, 2166−2171

Single crystals of **1′** were obtained by heating **1·g** from room temperature to 110 °C at a rate of 0.2 °C·min^{-1} and kept for 15 min under N_2 atmosphere and then cooled down to room temperature.[22,51] Single-crystal X-ray diffraction analysis revealed that **1′** keeps the same $R\bar{3}$ space group, but the unit-cell volume shrinks by 8.5% including 0.7% and 7.2% along the *a*/*b*-axis and *c*-axis, respectively (Table S1). After guest removal, the Zn−N bond distances (2.002(3) Å and 2.008(3) Å) slightly increase, the distorted tetrahedron coordination geometry becomes more regular (N−Zn−N/O−Zn−O/N−Zn−O 106.0(1)°−113.4(1)°), and the hydrogen bonds become stronger (N−H···O 2.682(4) Å and 2.709(7) Å). Nevertheless, the most remarkable structural change is found at one of the two independent organic ligands, in which the dihedral angles between the phenyl and pyrazole rings significantly increase by 30.5° (Figure 2c). Consequently, the widest and narrowest diameters of channel A are narrowed to 4.7 and 4.3 Å, respectively, while channel B has turned into 0D pore with a cross section area of 1.8 × 4.9 Å^2 (Figure 2b). As a result, the void ratio of **1′** was reduced to 25.4%.

Porosity Characterization. N_2 sorption isotherm of **1′** measured at 77 K reveals three consecutive steps with saturation uptakes of 135, 217, and 232 cm^3/g at p/p_0 = 0.0041, 0.044, and 0.20, corresponding to pore volumes of 0.211, 0.339, and 0.363 cm^3/g, respectively (Figure 3a). At p/p_0 = 0.20−0.99, the uptake gradually increases to 266 cm^3/g, giving a pore volume of 0.414 cm^3/g. For comparison, the crystallographic pore volumes of **1′** and **1** can be empirically calculated as 0.214 and 0.342 cm^3/g, respectively. Therefore, at the first adsorption step N_2 molecules fill up all the pores of **1′**. The second adsorption step reveals a framework expansion from **1′** to the original host framework of **1·g**. The third adsorption step and the latter gradual increase of uptake indicate that the coordination framework can further expand to a more porous state.

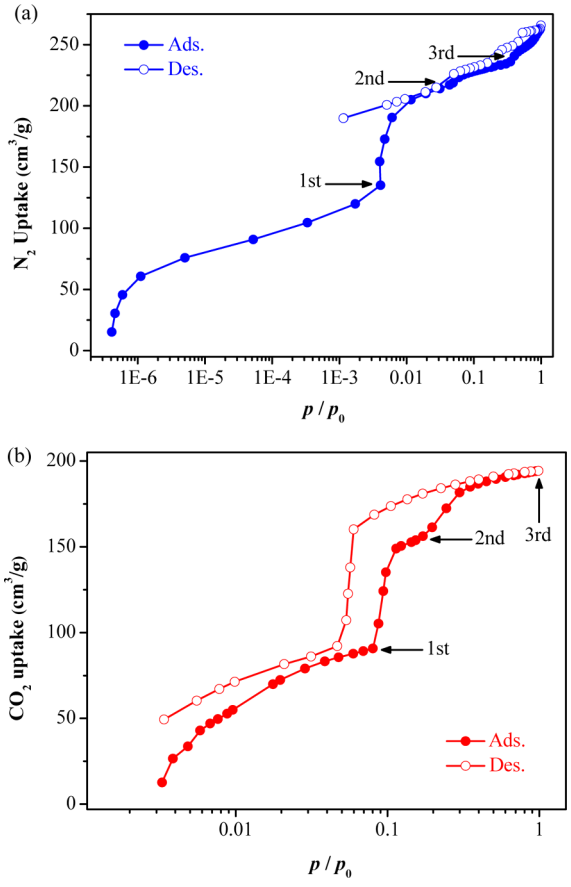

Figure 3. (a) N_2 (77 K) and (b) CO_2 (195 K) sorption isotherms of **1′**. The isotherm plateaus are marked by arrows.

CO_2 sorption isotherm of **1′** measured at 195 K also exhibits three consecutive adsorption steps with saturation uptakes of 90, 156, and 194 cm^3/g, corresponding to the pore volumes of 0.161, 0.279, and 0.346 cm^3/g, at p/p_0 = 0.080, 0.17, and 0.98, respectively (Figure 3b). The three pore volumes derived from the CO_2 isotherm steps may arise from the same adsorption and framework expansion phenomena of the N_2 isotherm, considering that they are all slightly smaller than those calculated from the crystal structure and from the N_2 isotherm. Because CO_2 has a relatively larger molecular volume and less regular molecular size compared with N_2, CO_2 can utilize the pore spaces less effectively at each state. It is also notable that the largest pore volume of the **dia** isomers calculated from the N_2 and CO_2 adsorption isotherms were only 0.20 and 0.18 cm^3/g, respectively,[46] being much smaller than those of **1′** (Table S2). The dissimilar stepped pressures and the absence of the gradually increase of CO_2 uptake after the third step demonstrate that **1′** can response differently toward different gases.

Sorption and Separation of C4 Hydrocarbons. Recovery of 1,3-butadiene from other C4 hydrocarbons is of great importance in petrochemical industry, on account of its widespread applications on preparation of synthetic rubbers.[52] Because of the very similar boiling points of *n*-butane (−0.5 °C), isobutane (−11.8 °C), *n*-butene (−6.5 °C), isobutene (−6.9 °C), and 1,3-butadiene (−4.5 °C),[48] conventional separation techniques such as distillation are rather difficult and energy-intensive. Recently, a few MOFs were studied for C4 hydrocarbon adsorption and separation.[48,53−56] Considering that the pore sizes of flexible **1′** are similar to the kinetic diameters of C4 hydrocarbons (*n*-butane: 4.7 Å, isobutane: 5.3 Å, *n*-butene: 4.5 Å, isobutene: 5.3 Å, 1,3-butadiene: 5.2 Å),[9] we investigated its potential for separation of C4 hydrocarbons. Sorption isotherms of C4 hydrocarbons measured at 303 K all exhibit gate-opening effects (Figure 4a). At ca. 0.0022−0.014 bar their uptakes suddenly rise, with gate-opening pressures following 1,3-butadiene < *n*-butene < *n*-butane < isobutene < isobutane. Obviously, this sequence does not match the kinetic diameters or boiling points of the C4 hydrocarbons. However, this sequence could be explained approximately by the difference of the smallest cross section areas of these molecules, for which the guest molecules tend to enter the pores by orienting their smallest cross sections to the pore apertures, and the smallest guest molecules can enter the pores easiest. The linear butadiene, butene, and butane have smaller molecular cross-section areas than the branched isobutene and isobutane molecules, and the molecules having more C=C double bonds and less C−C single bonds also have the smaller molecular cross section areas. After the gate-opening steps, the isotherms reach saturation with uptakes ca. 3.1, 2.8, and 2.4 mmol/g for 1,3-butadiene, isobutene/*n*-butene, and *n*-butane/isobutane, respectively, being consistent with their different molecular sizes/volumes (1,3-butadiene: 40.8 Å^3, isobutene: 44.3 Å^3, *n*-butene: 44.4 Å^3, *n*-butane: 47.8 Å^3, isobutane: 47.8 Å^3).[48]

To study the adsorption selectivities and separation performances for C4 hydrocarbons, a breakthrough simulation for equimolar 5-component *n*-butane/isobutane/*n*-butene/isobu-

DOI: 10.1021/acs.cgd.7b00100
Cryst. Growth Des. 2017, 17, 2166−2171

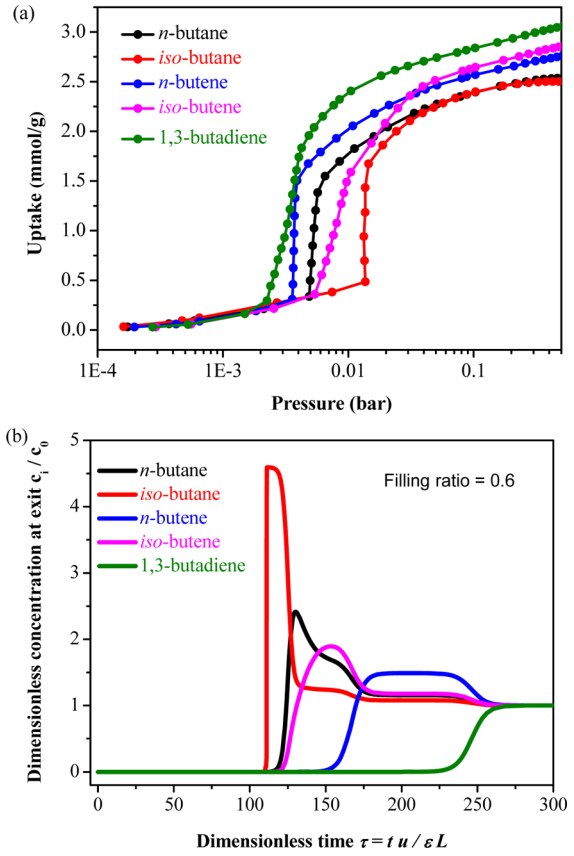

Figure 4. (a) C4 hydrocarbon adsorption isotherms for **1′** measured at 303 K and (b) simulated breakthrough curves for equimolar 5-component mixture of C4 hydrocarbons at 100 kPa and 303 K.

tene/1,3-butadiene mixture in **1′** at 100 kPa and 303 K was performed (Figure 4b and Table S3). As expected, the elution sequence is consistent with the trend of their gate-opening pressures, in which isobutane breakthroughs first and 1,3-butadiene breakthroughs last. After the adsorption equilibrium was reached (at dimensionless time $\tau > 270$), the amounts of isobutane/*n*-butane/isobutene/*n*-butene/1,3-butadiene adsorbed by **1′** can be calculated as 1/1.65/1.96/2.96/5.69.

CONCLUSIONS

Various structures have already been synthesized from the Zn(II)-H_2mpba system, including three supramolecular isomers of [Zn(Hmpba)$_2$] (α, β, and γ) possessing the 4-fold interpenetrated **dia** topology. In this work, we synthesized a new [Zn(Hmpba)$_2$] isomer (δ) showing a rare **afw** topology, larger porosity, and better single-crystallinity for investigation of its framework flexibility, by using toluene as a template. Moreover, the **afw** isomer shows dissimilar framework flexibilities and/or gate-opening pressures toward different gas molecules, which can be used for selective adsorption of 1,3-butadiene from C4 hydrocarbons.

ASSOCIATED CONTENT

Supporting Information

The Supporting Information is available free of charge on the ACS Publications website at DOI: 10.1021/acs.cgd.7b00100.

Table S1. Crystallographic data and structure refinement details; Table S2. Key parameters of the four [Zn(Hmpba)$_2$] isomers; C4 calculations and theoretical simulations (PDF)

Accession Codes

CCDC 1528960−1528961 contain the supplementary crystallographic data for this paper. These data can be obtained free of charge via www.ccdc.cam.ac.uk/data_request/cif, or by emailing data_request@ccdc.cam.ac.uk, or by contacting The Cambridge Crystallographic Data Centre, 12 Union Road, Cambridge CB2 1EZ, UK; fax: +44 1223 336033.

AUTHOR INFORMATION

Corresponding Authors

*(J.-P.Z.) E-mail: zhangjp7@mail.sysu.edu.cn.
*(X.-M.C.) E-mail: cxm@mail.sysu.edu.cn.

ORCID

Jie-Peng Zhang: 0000-0002-2614-2774

Author Contributions

#Z.-M.Y. and C.-T.H. contributed equally.

Notes

The authors declare no competing financial interest.

ACKNOWLEDGMENTS

This work was supported by the "973 Project" (2014CB845602), NSFC (21225105, 21290173, and 21473260), National Key Scientific Instrument and Equipment Development Project (2013YQ24051107), and National Postdoctoral Program for Innovative Talents (BX201600195).

REFERENCES

(1) Lee, J.; Farha, O. K.; Roberts, J.; Scheidt, K. A.; Nguyen, S. T.; Hupp, J. T. *Chem. Soc. Rev.* **2009**, *38*, 1450−1459.
(2) Liu, J.; Chen, L.; Cui, H.; Zhang, J.; Zhang, L.; Su, C.-Y. *Chem. Soc. Rev.* **2014**, *43*, 6011−6061.
(3) Huang, G.; Chen, Y.; Jiang, H. *Huaxue Xuebao* **2016**, *74*, 113−129.
(4) An, J.; Geib, S. J.; Rosi, N. L. *J. Am. Chem. Soc.* **2009**, *131*, 8376−8377.
(5) Levine, D. J.; Runčevski, T.; Kapelewski, M. T.; Keitz, B. K.; Oktawiec, J.; Reed, D. A.; Mason, J. A.; Jiang, H. Z. H.; Colwell, K. A.; Legendre, C. M.; FitzGerald, S. A.; Long, J. R. *J. Am. Chem. Soc.* **2016**, *138*, 10143−10150.
(6) Huxford, R. C.; Della Rocca, J.; Lin, W. *Curr. Opin. Chem. Biol.* **2010**, *14*, 262−268.
(7) Sun, C.-Y.; Qin, C.; Wang, C.-G.; Su, Z.-M.; Wang, S.; Wang, X.-L.; Yang, G.-S.; Shao, K.-Z.; Lan, Y.-Q.; Wang, E.-B. *Adv. Mater.* **2011**, *23*, 5629−5632.
(8) McKinlay, A. C.; Xiao, B.; Wragg, D. S.; Wheatley, P. S.; Megson, I. L.; Morris, R. E. *J. Am. Chem. Soc.* **2008**, *130*, 10440−10444.
(9) Li, J.-R.; Kuppler, R. J.; Zhou, H.-C. *Chem. Soc. Rev.* **2009**, *38*, 1477−1504.
(10) Qiu, S.; Xue, M.; Zhu, G. *Chem. Soc. Rev.* **2014**, *43*, 6116−6140.
(11) Barea, E.; Montoro, C.; Navarro, J. A. R. *Chem. Soc. Rev.* **2014**, *43*, 5419−5430.
(12) Tu, B.; Pang, Q.; Wu, D.; Song, Y.; Weng, L.; Li, Q. *J. Am. Chem. Soc.* **2014**, *136*, 14465−14471.
(13) He, H.; Sun, F.; Ma, S.; Zhu, G. *Inorg. Chem.* **2016**, *55*, 9071−9076.
(14) Cui, X.; Chen, K.; Xing, H.; Yang, Q.; Krishna, R.; Bao, Z.; Wu, H.; Zhou, W.; Dong, X.; Han, Y.; Li, B.; Ren, Q.; Zaworotko, M. J.; Chen, B. *Science* **2016**, *353*, 141−144.
(15) Zhang, S.-Y.; Zhang, X.; Li, H.; Niu, Z.; Shi, W.; Cheng, P. *Inorg. Chem.* **2015**, *54*, 2310−2314.
(16) Zhang, X.; Chen, W.; Shi, W.; Cheng, P. *J. Mater. Chem. A* **2016**, *4*, 16198−16204.

DOI: 10.1021/acs.cgd.7b00100
Cryst. Growth Des. 2017, 17, 2166−2171

(17) Luebke, R.; Weseliński, Ł. J.; Belmabkhout, Y.; Chen, Z.; Wojtas, Ł.; Eddaoudi, M. *Cryst. Growth Des.* **2014**, *14*, 414−418.
(18) Zhang, Y.-B.; Furukawa, H.; Ko, N.; Nie, W.; Park, H. J.; Okajima, S.; Cordova, K. E.; Deng, H.; Kim, J.; Yaghi, O. M. *J. Am. Chem. Soc.* **2015**, *137*, 2641−2650.
(19) Fu, H. R.; Wang, F.; Zhang, J. *Dalton Trans.* **2015**, *44*, 2893−2896.
(20) Lin, J.-M.; He, C.-T.; Liu, Y.; Liao, P.-Q.; Zhou, D.-D.; Zhang, J.-P.; Chen, X.-M. *Angew. Chem., Int. Ed.* **2016**, *55*, 4674−4678.
(21) Eddaoudi, M.; Kim, J.; Rosi, N.; Vodak, D.; Wachter, J.; Keeffe, M.; Yaghi, O. M. *Science* **2002**, *295*, 469−472.
(22) Zhang, J.-P.; Liao, P.-Q.; Zhou, H.-L.; Lin, R.-B.; Chen, X.-M. *Chem. Soc. Rev.* **2014**, *43*, 5789−5814.
(23) Nijem, N.; Wu, H.; Canepa, P.; Marti, A.; Balkus, K. J.; Thonhauser, T.; Li, J.; Chabal, Y. J. *J. Am. Chem. Soc.* **2012**, *134*, 15201−15204.
(24) Wu, X.; Niknam Shahrak, M.; Yuan, B.; Deng, S. *Microporous Mesoporous Mater.* **2014**, *190*, 189−196.
(25) Remy, T.; Baron, G. V.; Denayer, J. F. M. *Langmuir* **2011**, *27*, 13064−13071.
(26) Aguado, S.; Bergeret, G.; Titus, M. P.; Moizan, V.; Nieto-Draghi, C.; Bats, N.; Farrusseng, D. *New J. Chem.* **2011**, *35*, 546−550.
(27) Hyun, S.-m.; Lee, J. H.; Jung, G. Y.; Kim, Y. K.; Kim, T. K.; Jeoung, S.; Kwak, S. K.; Moon, D.; Moon, H. R. *Inorg. Chem.* **2016**, *55*, 1920−1925.
(28) Chae, S. H.; Kim, H.-C.; Lee, Y. S.; Huh, S.; Kim, S.-J.; Kim, Y.; Lee, S. J. *Cryst. Growth Des.* **2015**, *15*, 268−277.
(29) Foo, M. L.; Matsuda, R.; Hijikata, Y.; Krishna, R.; Sato, H.; Horike, S.; Hori, A.; Duan, J.; Sato, Y.; Kubota, Y.; Takata, M.; Kitagawa, S. *J. Am. Chem. Soc.* **2016**, *138*, 3022−3030.
(30) Wang, J.; Krishna, R.; Yang, T.; Deng, S. *J. Mater. Chem. A* **2016**, *4*, 13957−13966.
(31) Li, Y.-W.; He, K.-H.; Bu, X.-H. *J. Mater. Chem. A* **2013**, *1*, 4186−4189.
(32) Hamon, L.; Llewellyn, P. L.; Devic, T.; Ghoufi, A.; Clet, G.; Guillerm, V.; Pirngruber, G. D.; Maurin, G.; Serre, C.; Driver, G.; Beek, W. v.; Jolimaître, E.; Vimont, A.; Daturi, M.; Férey, G. *J. Am. Chem. Soc.* **2009**, *131*, 17490−17499.
(33) Schneemann, A.; Bon, V.; Schwedler, I.; Senkovska, I.; Kaskel, S.; Fischer, R. A. *Chem. Soc. Rev.* **2014**, *43*, 6062−6096.
(34) Pachfule, P.; Das, R.; Poddar, P.; Banerjee, R. *Cryst. Growth Des.* **2011**, *11*, 1215−1222.
(35) Chen, Z.; Xiang, S.; Zhao, D.; Chen, B. *Cryst. Growth Des.* **2009**, *9*, 5293−5296.
(36) He, Y.-P.; Tan, Y.-X.; Zhang, J. *Cryst. Growth Des.* **2013**, *13*, 6−9.
(37) Jia, Y.-Y.; Ren, G.-J.; Li, A.-L.; Zhang, L.-Z.; Feng, R.; Zhang, Y.-H.; Bu, X.-H. *Cryst. Growth Des.* **2016**, *16*, 5593−5597.
(38) Catarineu, N. R.; Schoedel, A.; Urban, P.; Morla, M. B.; Trickett, C. A.; Yaghi, O. M. *J. Am. Chem. Soc.* **2016**, *138*, 10826−10829.
(39) Schoedel, A.; Li, M.; Li, D.; O'Keeffe, M.; Yaghi, O. M. *Chem. Rev.* **2016**, *116*, 12466−12535.
(40) Moulton, B.; Zaworotko, M. J. *Chem. Rev.* **2001**, *101*, 1629−1658.
(41) James, S. L. *Chem. Soc. Rev.* **2003**, *32*, 276−288.
(42) Robin, A. Y.; Fromm, K. M. *Coord. Chem. Rev.* **2006**, *250*, 2127−2157.
(43) Makal, T. A.; Yakovenko, A. A.; Zhou, H.-C. *J. Phys. Chem. Lett.* **2011**, *2*, 1682−1689.
(44) Heering, C.; Boldog, I.; Vasylyeva, V.; Sanchiz, J.; Janiak, C. *CrystEngComm* **2013**, *15*, 9757−9768.
(45) He, C.-T.; Tian, J.-Y.; Liu, S.-Y.; Ouyang, G.; Zhang, J.-P.; Chen, X.-M. *Chem. Sci.* **2013**, *4*, 351−356.
(46) He, C.-T.; Liao, P.-Q.; Zhou, D.-D.; Wang, B.-Y.; Zhang, W.-X.; Zhang, J.-P.; Chen, X.-M. *Chem. Sci.* **2014**, *5*, 4755−4762.
(47) Bryant, M. R.; Burrows, A. D.; Fitchett, C. M.; Hawes, C. S.; Hunter, S. O.; Keenan, L. L.; Kelly, D. J.; Kruger, P. E.; Mahon, M. F.; Richardson, C. *Dalton Trans.* **2015**, *44*, 9269−9280.
(48) Kishida, K.; Okumura, Y.; Watanabe, Y.; Mukoyoshi, M.; Bracco, S.; Comotti, A.; Sozzani, P.; Horike, S.; Kitagawa, S. *Angew. Chem., Int. Ed.* **2016**, *55*, 13784−13788.
(49) Foces-Foces, C.; Cativiela, C.; Zurbano, M. M.; Sobrados, I.; Jagerovic, N.; Elguero, J. *J. Chem. Crystallogr.* **1996**, *26*, 579−584.
(50) Zhang, R. C.; Wang, J. J.; Yuan, B. Q.; Zhang, J. C.; Zhou, L.; Wang, H. B.; Zhang, D. J.; An, Y. L. *Inorg. Chem.* **2016**, *55*, 11593−11599.
(51) Liu, J.-L.; Liu, W.; Huang, G.-Z.; Tong, M.-L. *Sci. Bull.* **2015**, *60*, 447−452.
(52) Liu, H.; He, Y.; Jiao, J.; Bai, D.; Chen, D.-l.; Krishna, R.; Chen, B. *Chem. - Eur. J.* **2016**, *22*, 14988−14997.
(53) Lange, M.; Kobalz, M.; Bergmann, J.; Lassig, D.; Lincke, J.; Mollmer, J.; Moller, A.; Hofmann, J.; Krautscheid, H.; Staudt, R.; Glaser, R. *J. Mater. Chem. A* **2014**, *2*, 8075−8085.
(54) Hähnel, T.; Kalies, G.; Krishna, R.; Möllmer, J.; Hofmann, J.; Kobalz, M.; Krautscheid, H. *Microporous Mesoporous Mater.* **2016**, *224*, 392−399.
(55) Li, B.; Belmabkhout, Y.; Zhang, Y.; Bhatt, P. M.; He, H.; Zhang, D.; Han, Y.; Eddaoudi, M.; Perman, J. A.; Ma, S. *Chem. Commun.* **2016**, *52*, 13897−13900.
(56) Bon, V.; Klein, N.; Senkovska, I.; Heerwig, A.; Getzschmann, J.; Wallacher, D.; Zizak, I.; Brzhezinskaya, M.; Mueller, U.; Kaskel, S. *Phys. Chem. Chem. Phys.* **2015**, *17*, 17471−17479.

DOI: 10.1021/acs.cgd.7b00100
Cryst. Growth Des. 2017, 17, 2166−2171

Supporting information

A New Isomeric Porous Coordination Framework Showing Single-crystal to Single-crystal Structural Transformation and Preferential Adsorption of 1,3-Butadiene from C4 Hydrocarbons

Zi-Ming Ye[a†], Chun-Ting He[a†], Yan-Tong Xu[†], Rajamani Krishna[‡], Yi Xie[†], Dong-Dong Zhou[†], Hao-Long Zhou[†], Jie-Peng Zhang[†]* and Xiao-Ming Chen[†]*

[†]*MOE Key Laboratory of Bioinorganic and Synthetic Chemistry, School of Chemistry, Sun Yat-Sen University, Guangzhou 510275, China*

[‡]*Van't Hoff Institute for Molecular Sciences, University of Amsterdam, Science Park 904, 1098 XH Amsterdam, The Netherlands*

[a]These authors contributed equally.

Table of contents

Table S1. Crystallographic data and structure refinement details

Complex	$[Zn(Hmpba)_2]\cdot 7/6C_7H_8\cdot 1/6CH_3OH$ (**1·g**)	$[Zn(Hmpba)_2]$ (**1'**)
Formula	$C_{32.33}H_{32}N_4O_{4.17}Zn$	$C_{24}H_{22}N_4O_4Zn$
Formula weight	608.65	495.85
Temperature (K)	123(2)	298(2)
Crystal system	Trigonal	Trigonal
Space group	*R*-3	*R*-3
a/Å	36.6350(14)	36.3927(7)
b/Å	36.6350(14)	36.3927(7)
c/Å	12.1278(9)	11.2519(3)
γ/°	120	120
V/Å^3	14096.3(17)	12905.5(7)
Z	18	18
D_c/g cm^{-3}	1.291	1.148
reflns coll.	28322	10668
unique reflns	6151	4333
R_{int}	0.0345	0.0156
R_1 [$I > 2\sigma(I)$][a]	0.0464	0.0463
wR_2 [$I > 2\sigma(I)$][b]	0.1231	0.1257
R_1 (all data)	0.0583	0.0571
wR_2 (all data)	0.1326	0.1350
GOF	1.032	1.035

[a] $R_1=\Sigma||F_o| - |F_c||/\Sigma|F_o|$. [b] $wR_2 =[\Sigma w(F_o^2 - F_c^2)^2/\Sigma w(F_o^2)^2]^{1/2}$.

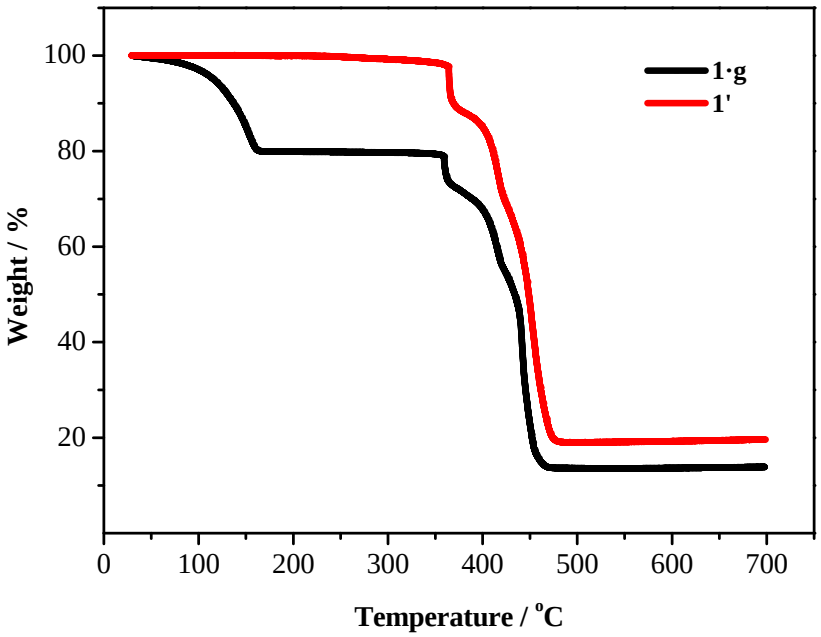

Figure S1. TG curves of **1·g** and **1'**.

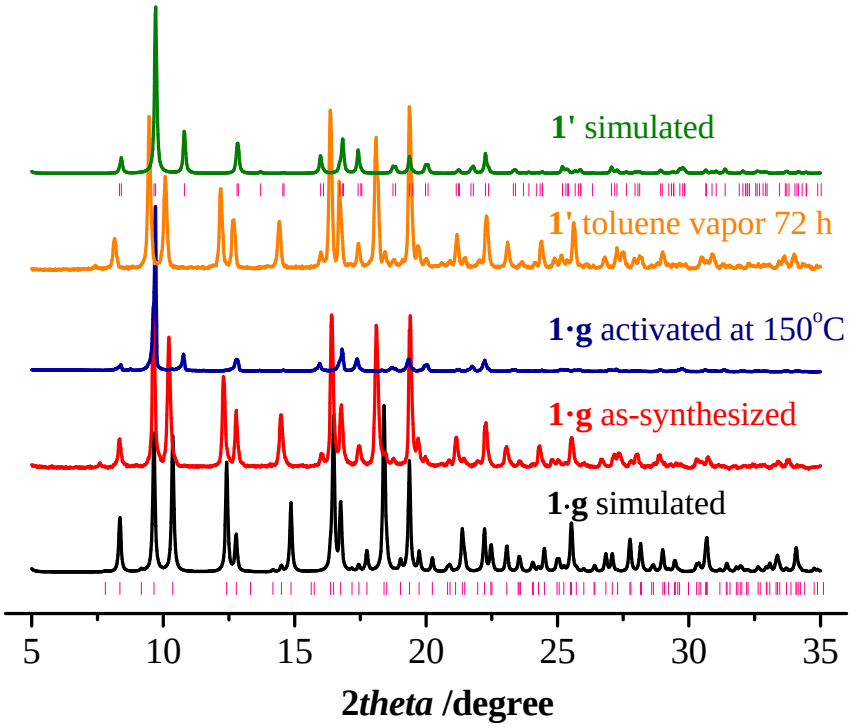

Figure S2. PXRD patterns of **1·g** and **1'**.

Table S2. Key parameters of the four [$Zn(Hmpba)_2$] isomers

Isomer notation	α	β	γ	δ
Solvent and templates	EtOH, H_2O, Dioxane	EtOH, H_2O	H_2O	MeOH, Toluene
Topology	**dia**	**dia**	**dia**	**afw**
Interpenetration type	Ia	IIb	Ia	IIIa
Void ratio / %	25.6	27.6	2.9	35.9
Crystal system	orthorhombic	Orthorhombic	Tetragonal	Trigonal
Space group	*Pba*2	*Fdd*2	$I4_1/acd$	*R*-3
Cell volume / $Å^3$	1361.25(14)	22513(4)	9077.2(11)	14096.3(17)
Density / g cm^{-3}	1.425	1.276	1.451	1.291
Crystallogrphic pore volume / cm^3 g^{-1}	0.180	0.216	0.020	0.278
Pore volume calculated from N_2 (77K) adsorption / cm^3 g^{-1}	0.06	0.20	Not measured	0.34
Pore volume calculated from CO_2 (195K) adsorption / cm^3 g^{-1}	0.15	0.18	Not measured	0.35
Reference	1	1	1	This work

C4 calculations and theoretical simulations

Fitting of experimental data on pure component isotherms

The isotherm data for *n*-butane, *iso*-butane, *n*-butene, *iso*-butene, and 1,3-butadiene, measured at 303 K in **1'** were fitted with the Dual-site Langmuir-Freundlich model individually for each temperature

$$q = q = q_{A,sat}\frac{b_A p^{\nu_A}}{1+b_A p^{\nu_A}} + q_{B,sat}\frac{b_B p^{\nu_B}}{1+b_B p^{\nu_B}} \quad (1)$$

The 2-site Langmuir-Freundlich parameters are provided in Table S2.

Table S3. 2-site Langmuir-Freundlich parameters for *n*-butane, *iso*-butane, *n*-butene; *iso*-butene, and 1,3-butadiene at 303 K in **1'**.

	Site A			Site B		
	$q_{i,A,sat}$ mol/kg	$b_{i,A}$ $Pa^{-\nu_i}$	$\nu_{i,A}$ dimensionless	$q_{i,B,sat}$ mol/kg	$b_{i,B}$ $Pa^{-\nu_i}$	$\nu_{i,B}$ dimensionless
n-C_4H_{10}	1.5	4.52×10^{-35}	12.5	1.2	3.79×10^{-03}	0.7
iso-C_4H_{10}	1.5	2.73×10^{-43}	13.4	1.1	4.28×10^{-03}	0.74
n-C_4H_8	1.6	2.20×10^{-47}	18	1.3	2.55×10^{-03}	0.76
iso-C_4H_8	0.95	3.21×10^{-47}	16	2	5.24×10^{-04}	1
1,3-C_3H_6	1.9	1.18×10^{-15}	5.9	1.2	1.26×10^{-03}	0.9

Transient breakthrough of mixtures in fixed bed adsorbers

The performance of industrial fixed bed absorbers is dictated by a combination of adsorption selectivity and uptake capacity. For a proper comparison of various MOFs, we perform transient breakthrough simulations using the simulation methodology described in the literature.[2, 3] For the breakthrough simulations, the following parameter values were used: length of packed bed, L = 0.3 m; voidage of packed bed, ε = 0.4; superficial gas velocity at inlet, u = 0.04 m/s. The transient breakthrough simulation results are presented in terms of a *dimensionless* time, τ, defined by dividing the actual time, t, by the characteristic time, $\frac{L\varepsilon}{u}$.

Notation

b_A	Langmuir-Freundlich constant for species i at adsorption site A, $Pa^{-\nu_{iA}}$
b_B	Langmuir-Freundlich constant for species i at adsorption site B, $Pa^{-\nu_{iB}}$
L	length of packed bed adsorber, m
p_i	partial pressure of species i in mixture, Pa
p_t	total system pressure, Pa
q_i	component molar loading of species i, mol kg^{-1}
Q_{st}	isosteric heat of adsorption, J mol^{-1}
t	time, s
T	absolute temperature, K
t	time, s
T	absolute temperature, K
u	superficial gas velocity in packed bed, m s^{-1}

Greek letters

ε	voidage of packed bed, dimensionless
ν	Freundlich exponent, dimensionless
ρ	framework density, kg m^{-3}
τ	time, dimensionless

Subscripts

i	referring to component *i*
t	referring to total mixture

References

(1) He, C.-T.; Liao, P.-Q.; Zhou, D.-D.; Wang, B.-Y.; Zhang, W.-X.; Zhang, J.-P.; Chen, X.-M. *Chem. Sci.* **2014**, 5, 4755-4762.

(2) Krishna, R. *Micropor. Mesopor. Mater.* **2014**, *185*, 30-50.

(3) Krishna, R. *RSC Adv.* **2015**, *5*, 52269-52295.